arXiv:0810.0190v3 [astro-ph] 10 Mar 2009

Dynamical Dark Energy simulations: high accuracy Power Spectra at high redshift

Luciano Casarini[1,2], **Andrea V. Macciò**[3], **Silvio A. Bonometto**[1,2]

[1]Department of Physics G. Occhialini – Milano–Bicocca University, Piazza della Scienza 3, 20126 Milano, Italy

[2]I.N.F.N., Sezione di Milano

[3]Max-Planck-Institut für Astronomie, Königstuhl 17, 69117 Heidelberg, Germany

Abstract. Accurate predictions on non–linear power spectra, at various redshift z, will be a basic tool to interpret cosmological data from next generation mass probes, so obtaining key information on Dark Energy nature. This calls for high precision simulations, covering the whole functional space of $w(z)$ state equations and taking also into account the admitted ranges of other cosmological parameters; surely a difficult task. A procedure was however suggested, able to match the spectra at $z = 0$, up to $k \sim 3\,h\mathrm{Mpc}^{-1}$, in cosmologies with an (almost) arbitrary $w(z)$, by making recourse to the results of N–body simulations with w = const. In this paper we extend such procedure to high redshift and test our approach through a series of N–body gravitational simulations of various models, including a model closely fitting WMAP5 and complementary data. Our approach detects w = const. models, whose spectra meet the requirement within 1 % at $z = 0$ and perform even better at higher redshift, where they are close to a permil precision. Available Halofit expressions, extended to (constant) $w \neq -1$ are unfortunately unsuitable to fit the spectra of the physical models considered here. Their extension to cover the desired range should be however feasible, and this will enable us to match spectra from any DE state equation.

PACS numbers: 98.80.-k, 98.65.-r

1. Introduction

There seems to be little doubt left that a Dark Energy (DE) component is required, to account for cosmological observables. Its first evidence came from the Hubble diagram of SNIa, showing an accelerated cosmic expansion, but a *flat* cosmology with $\Omega_m \simeq 0.25$, $\Omega_b \simeq 0.04$ and $h \simeq 0.7$ is now required by CMB and LSS data and this implies that the gap between Ω_m and unity is to be filled by a smooth non–particle component (Ω_m, Ω_b: matter, baryon present density parameters; h: present Hubble parameter in units of 100 km/s/Mpc; CMB: cosmic microwave background; LSS: large scale structure; for SNIa data see [1, 2]; updated cosmological parameters, taking into account most available data, are provided within the context of WMAP5 release [3].

If DE evidence seems sound, its nature is perhaps the main puzzle of cosmology. Aside of a cosmological constant Λ, possibly related to vacuum energy, and a scalar self–interacting field ϕ, various pictures have been recently discussed, ranging from a supposed back–reaction of inhomogeneity formation to GR modifications and including even more exotic alternatives (see, *e.g.*, [6]). However, in most of these cases, a DE component, with a suitable $w(a)$ state parameter (a: scale factor), can still be an *effective* description, and a number of observational projects have been devised, aiming first of all at constraining $w(a)$ (among them let us quote the DUNE–EUCLIDE project [7]). Some of them are likely to be realized in the next decade(s) and, to interpret their outcomes, we need accurate predictions on selected observables. In particular, it has been outlined [8] that, to fully exploit weak lensing surveys, we need predictions on non–linear power spectra, accurate up to $\sim 1\%$.

N–body gravitational simulations safely predict non–linear matter evolution up to wavenumbers $k \simeq 3\,h\,\mathrm{Mpc}^{-1}$. When the scale of galaxy clusters is approached, discrepancies from hydrodynamical simulations, although small, exceed a few percents [9, 10, 11]: too much for the accuracy required. Within the above range, safe expressions of matter fluctuation spectra at $z = 0$, for any state equation $w(a)$, can be obtained from simulations of suitable models with $w = \text{const.}$. This paper extends the technique yielding such expressions, so to include higher redshift z, where they will be mostly needed.

A fair approximation to the mass power spectrum for ΛCDM models is the *Halofit* expression [12], based on the halo model of structure formation and using numerical simulations to fix parameters left free by the theoretical analysis. Halofit expressions were extended [13] to include cosmologies with a constant state parameter ($-1.5 < w < -0.5$) and for a fairly wide range of the parameters Ω_c, Ω_b, h, n_s, σ_8 (here n_s : primeval spectral index for scalar fluctuations; σ_8 : linear r.m.s. fluctuation amplitude on the scale of $8\,h^{-1}$Mpc). To this aim suitable n–body simulations, in a box of size $L_{box} = 110\,h^{-1}$Mpc and with force resolution $\epsilon = 143\,h^{-1}$kpc, were run.

We tentatively applied such generalized Halofit expressions to our cases. Unfortunately, soon above rather low z's, they fail to work. This is not unexpected, as we had been pushing them outside the expected range of validity. Among the models

considered, however, there are cosmologies closely fitting WMAP5 and complementary data. Accordingly, further work will be needed to provide suitable generalized Halofit expressions.

Dynamical Dark Energy (dDE) simulations, with a variable state parameter $w(a)$ deduced from scalar field potentials admitting a tracker solutions, have been performed since 2003 [14] (see also [15, 16, 17]) and compared with $w = const$ simulation outputs. Observables considered in these papers, however, only marginally included spectra. In a recent work ([18] FLL hereafter), however, it has been shown how spectral predictions for constant–w models can also be used to fit the spectra of cosmologies with a state parameter

$$w(a) = w_o + (1 - a)w_a \ , \tag{1}$$

given by a first degree polynomial.

In fact, it had been known since several years that spectra at a given (low) redshift $\bar{z}$ mainly depends on the comoving distance between $\bar{z}$ and the last scattering band ($d_{LSB}(\bar{z})$), at least for models where baryons and CDM are the only matter components with a ratio not too far from canonical values [19]. Aiming at 1 % accuracy, FLL seek the constant–w model which grants the same distance from LSB of an assigned $w(a)$ function, without varying any other parameter, and claim that spectral differences between the two models are at the per–mil level for $k < 1\,h$ Mpc^{-1}, but still at the percent level for $k < 3\,h$ Mpc^{-1}, at $z = 0$.

On this basis, at $z = 0$, one could think to use the *Halofit* extension provided in [13] to predict the spectra of models with variable w, in a large number of cases.

FLL started from models with a constant equation of state ($w = -K$, with $K = 0.9, 1, 1.1$), for which the distance from the LSB is $d^{(K)}_{LSB}(z)$, and then compared them with variable–w models with the same distance from the LSB at redshift zero: $d_{LSB}(0) = d^{(K)}_{LSB}(0)$. In the attempt to extend the fit between spectra from $z = 0$ to higher z, they just renormalize the amplitudes of the constant–w model spectra at higher redshift, so to meet the low–k linear behavior of the variable–w models. This technique allows them to reduce spectral discrepancies, in average still below 1 %, but attaining a maximum of a few percents at larger k's.

Here we shall bypass this renormalization procedure, aiming at the per–mil precision for any z. To this end we extend directly the criterion suggested in [19] to any redshift, suitably seeking a constant–w model such that $d_{LSB}(z)/d^{(K)}_{LSB}(z) \equiv 1$, z by z (allowing, of course, for any value of K). This also requires to follow the variations of model parameters through their evolution dictated by the assigned $w(z)$. Two options to do so will be outlined and we shall test the procedure of the simpler option through a number of N–body simulations.

The remainder of this paper is organized as follows. Section 2 is devoted to briefly illustrate such dDE model. In Section 4 we present our numerical simulations and their analysis. Section 5 contains our results on the Power Spectrum and a short discussion on them. Finally in Section 6 we present our main conclusions.

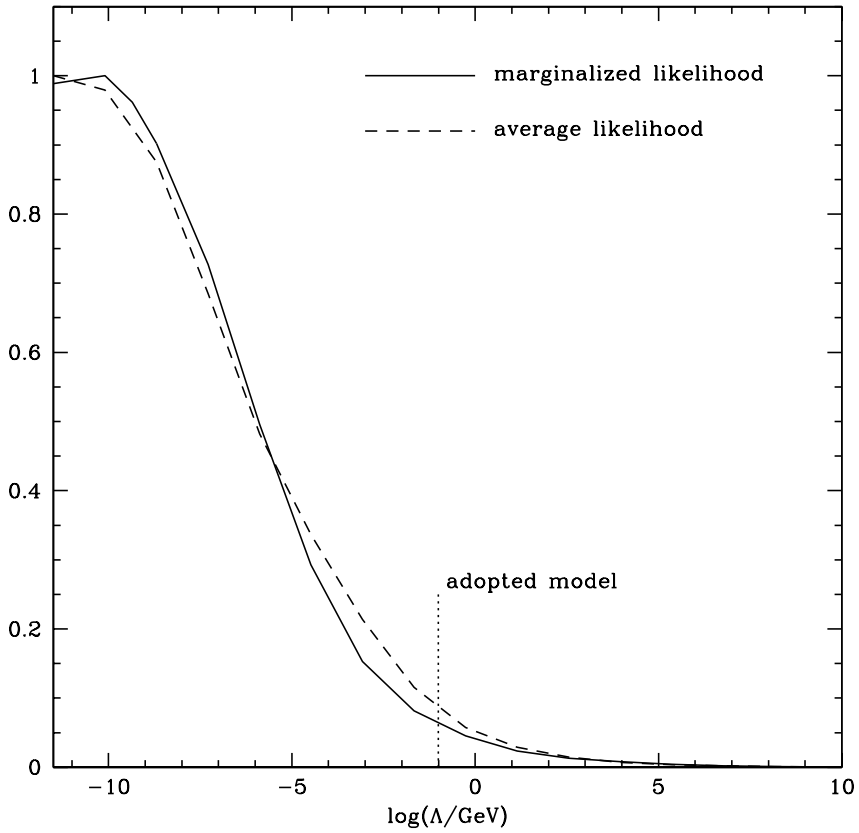

Figure 1. Likelihood distribution on $\log\Lambda$ for SUGRA cosmologies.

2. The models considered

In this paper we run a series of simulations for two cosmological models: (i) a model where $w(a)$ is a polynomial (1); (ii) a SUGRA model. The former model is selected to coincide with one of the models considered by FLL, so to allow a close comparison of the outputs.

SUGRA models are an alternative example of faster varying state equation; they are true dDE model, where DE is a scalar field ϕ, self–interacting through a SUGRA potential

$$V(\phi) = (\Lambda^{\alpha+4}/\phi^{\alpha})\exp(4\pi\phi^2/m_p^2) \tag{2}$$

admitting tracker solutions [20, 21, 22]. Here: $m_p = G^{-1/2}$ is the Planck mass; Λ and α are suitable parameters; however, in a spatially flat cosmology, once the present DE density parameter is assigned, either of them is fixed by the other one. Here we shall define our SUGRA model through the value of Λ $(= 0.1\mathrm{GeV})$

In fact, a fit of SUGRA with data, based on MCMC (MonteCarlo Markov Chains), was recently obtained by [5]. Data include WMAP5 outputs on anisotropies and polarization [3], SNIa [1] and 2dF data [4] on matter fluctuation spectra (including therefore the BAO position). In Figure 1 we exhibit the likelihood distribution on the parameter $\log(\Lambda/\mathrm{GeV})$, obtained from the fit. Using $\Lambda = 0.1$ GeV is a compromise

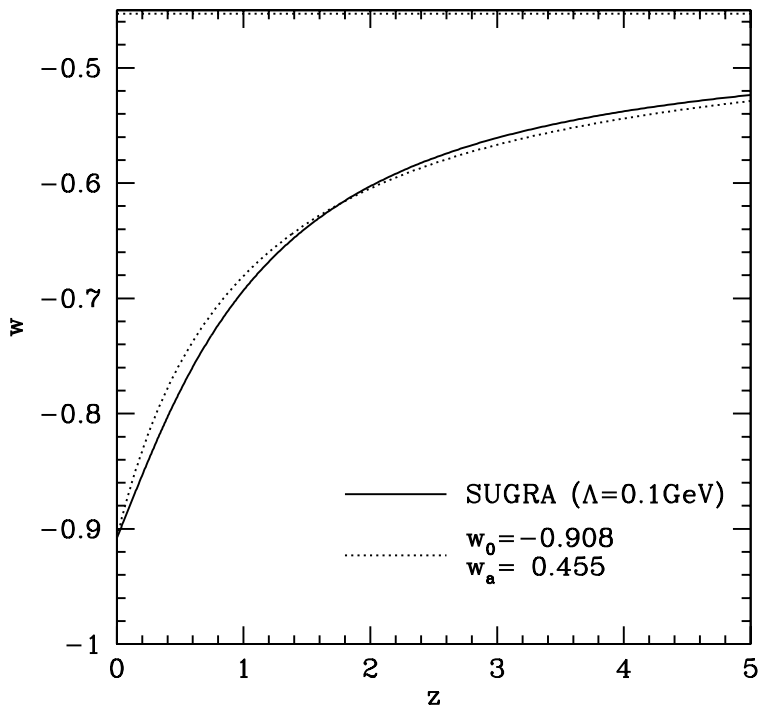

Figure 2. Evolution of the state parameter w for the SUGRA model used in the simulation ($\Lambda = 0.1$), compared with the closest polynomial $w(a)$.

between top likelihood and a physically significant Λ . The values of the other parameters in the SUGRA simulation are then chosen quite close to the best–fit obtained once $\Lambda = 0.1$ GeV is fixed, and are reported in Table 1. The evolution with the redshift of the state parameter for this model is shown in Figure 2 and compared with a polynomial $w(a)$ ($w_o = -0.908$, $w_a = 0.455$) coinciding with SUGRA at $z = 0$ and $z = 10$. In general, the redshift dependence of the SUGRA state parameter can only be approached by an expression of the form (1). However, just looking at the recent WMAP results [3],we see that these w_o, w_a are at $\sim 1.5\,\sigma$'s from the best–fit polynomial parameters.

In Table 1 we give the $z = 0$ parameters of the two variable–w models considered.

Table 1

	Ω_c	Ω_b	h	σ_8	n_s
polynom. :	0.193	0.041	0.74	0.76	0.96
SUGRA	0.209	0.046	0.70	0.75	0.97

Let us remind that the former model is selected mostly for the sake of comparison. Its polynomial coefficient read $w_o = -0.8$, $w_a = -0.732$ and it is characterized by a rather low likelihood with respect to data (see [3])

In Figure 3 we show the behavior of the linear growth factor $G(z)$ for both models, normalized to the growth factor in the constant–w model yielding the same $d_{LSB}(z = 0)$; *i.e.*, for the SUGRA model, $w = -0.7634$; for the polynomial model, as already

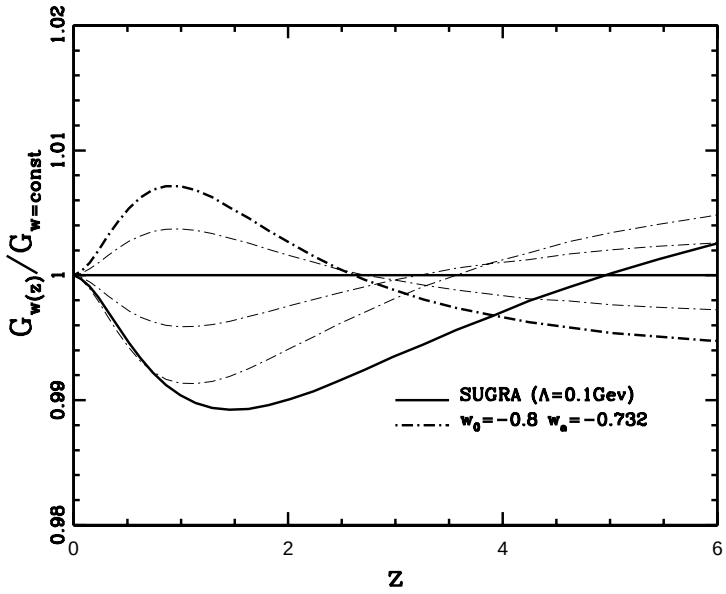

Figure 3. Linear growth factors for different models, compared with the growth factor of the constant–w model fitting them at $z = 0$. Besides of the models treated in detail in this work (indicated in the frame), we also show the growth factors for a further set of models treated by FLL (see text).

mentioned, $w = -1$. For the sake of comparison we report $G(z)$ for a few other models, whose $d_{LSB}(z = 0)$ also coincides with ΛCDM (in these models w_o and w_a hold -1.2, -1.1, -0.9 and 0.663, 0.341, -0.359, respectively). $G(z)$ is then the renormalizing factor for the spectrum at redshift z in the FLL approach. Spectra worked out with FLL technique will be better where $G_{w(z)}/G_{w=-1}$ is smaller. We notice that, for each model, there exist a *crossover* redshift z_{co}, such that $G(z_{co})$ coincides with the growth factor of ΛCDM. At this redshift, the FLL procedure does not require renormalization.

3. Variable vs. constant w

In order to find a constant–w model whose spectrum approaches dDE at a redshift $z \neq 0$, one first computes the distance $d_{LSB}(z)$, from z to the LSB, in the model $\mathcal{M}$ considered. At such redshift z, cosmological parameters as Ω_b, Ω_c, h, σ_8 no longer keep their $z = 0$ values. However, one can easily calculate them and find a constant–w model whose parameters at that z are $\Omega_b(z)$, $\Omega_c(z)$, $h(z)$, $\sigma_8(z)$ and coincide with the values in $\mathcal{M}$. In such model, then, the $z = 0$ values of the parameters will be different from their values in $\mathcal{M}$. Such model is then expected to have a non–linear spectrum closely approaching $\mathcal{M}$ at z, just as FLL found at $z = 0$. The models defined in this way shall clearly be different for different z and will be said to satisfy to the *strong requirement*.

Among other difficulties, making use of such models to approximate high–z spectra causes a technical problem which stands on the way to test this approach through simulations. Let L be the side of the box to be used. As already outlined, for the $\mathcal{M}$ and constant–w models, the $z = 0$ values of h are different; therefore, if we take equal

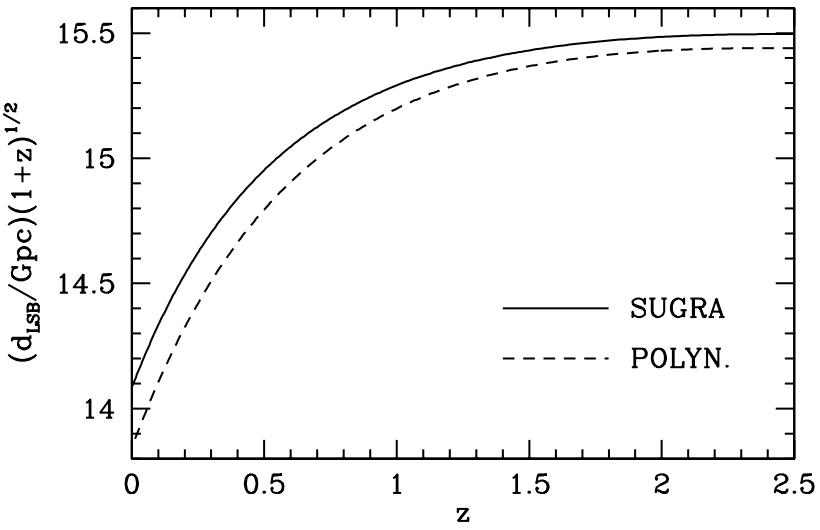

Figure 4. Distance between z and the LSB in the SUGRA and polynomial models of Table 1 ($\mathcal{M}$ models).

values for Lh (or L measured in h^{-1}Mpc) we shall have different L values. A similar problem occurs when we normalize, as the r.m.s. fluctuation amplitude σ_8 refers to the h dependent scale of $8\,h^{-1}$Mpc. All that induces quite a few complications, if we aim at comparing fairly normalized spectra of different models, with the same seed and the same wavenumber contributions.

This difficulty can be soon overcame if we replace the above strong requirement with the *weak requirement* we shall now define. Let us first notice that, being

$$H^2 = \frac{8\pi}{3} G\rho_{cr} = \frac{8\pi}{3} G\rho_m \Omega_m^{-1} \tag{3}$$

at any redshift, $\Omega_m h^2$ however scales as a^{-3}, independently of DE nature. Accordingly, a constant–w model whose $z = 0$ values of Ω_b, Ω_c and h^2 coincide with those of $\mathcal{M}$, will share with it the values of the reduced density parameters $\omega_b = \Omega_b h^2$ and $\omega_c = \Omega_c h^2$ at any redshift (attention is to be payed, all through this paper, to the different meanings of the symbols w and ω, respectively state parameter and reduced density parameters). In order to have the same $d_{LSB}(z)$, of course, it shall have a different $h(z)$, that we however do not need to evaluate explicitly. What we need to know are the value of the *constant* $w(z)$ as well as the value $\sigma_8(z)$, to be assigned to the r.m.s. fluctuation amplitude at $z = 0$, to meet the $\mathcal{M}$ value of σ_8 at z.

In this paper we shall test this weak requirement (W.R.) that the dDE model $\mathcal{M}$ and the *auxiliary* model $\mathcal{W}(z)$ have equal $d_{LSB}(z)$, σ_8, ω_c and ω_b, while h is chosen with an *ad–hoc* criterion, yielding a z–independent h at $z = 0$.

In Figures 4, 5, 6 we report the distance from the LSB $d_{LSB}(z)$, as well as the values

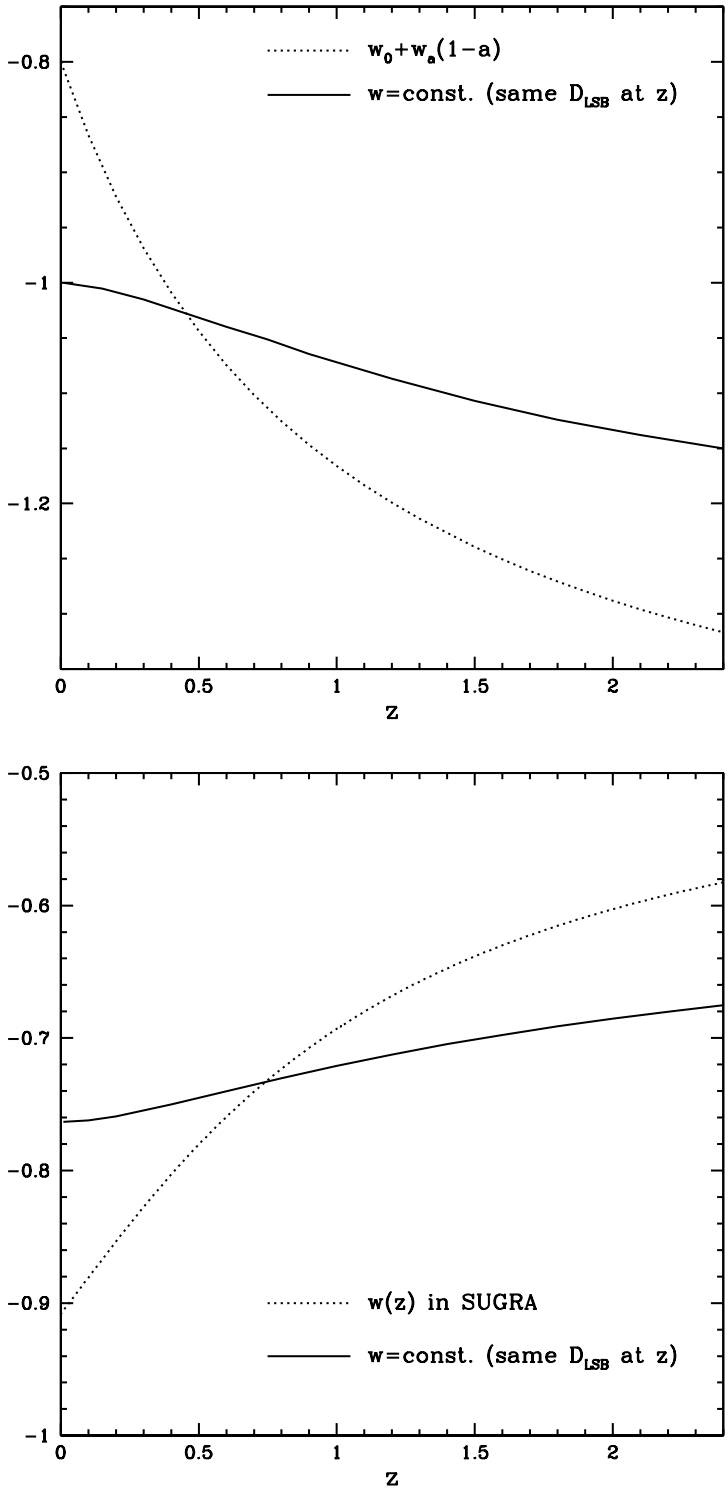

Figure 5. State parameter of the auxiliary models, as a function of redshift. For the sake of comparison, also the intrinsic $w(z)$ dependence of each $\mathcal{M}$ model is shown.

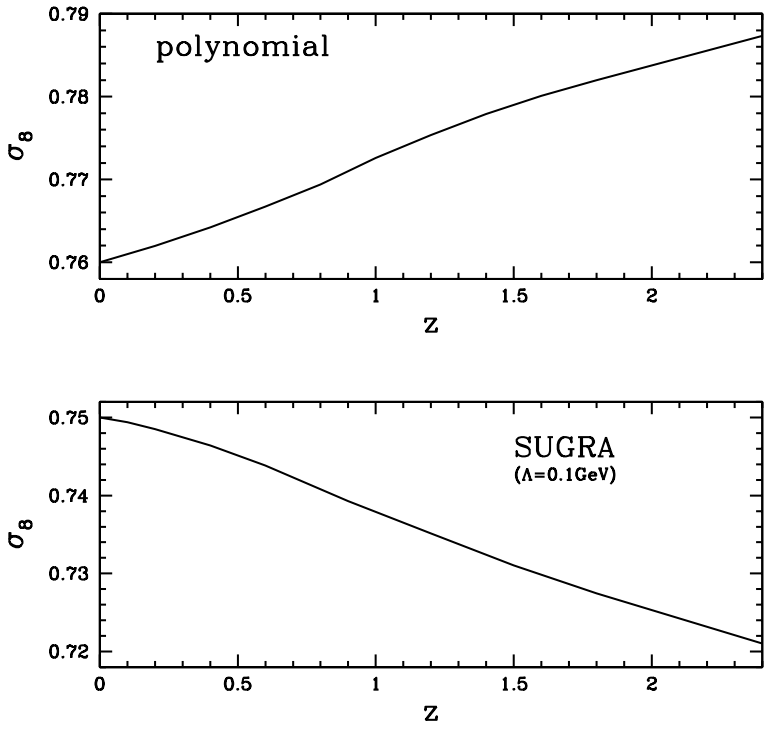

Figure 6. Values of σ_8 at $z = 0$ for constant–w models whose r.m.s. fluctuation amplitude meets the σ_8 value of the $\mathcal{M}$ model at z.

of $w(z)$ and $\sigma_8(z)$ for the auxiliary models $\mathcal{W}(z)$ defined according to the W.R. .

FLL had been seeking an auxiliary model only at $z = 0$, making recourse to a different treatment at greater redshift, claimed to grant a precision $\mathcal{O}(2$–$3\%)$. As we shall see, seeking an auxiliary model at any redshift, according to the W.R., allows a precision ~ 10 times better in the relevant k range and does not lead to numerical complications. The goal would be complete if such models were in the parameter ranges considered by generalized Halofit expressions [13] (at $z = 0$): $0.211 < \Omega_m < 0.351$, $0.041 < \Omega_b < 0.0514$, $0.644 < h < 0.776$, $0.800 < \sigma_8 < 0.994$, $0.915 < n_s < 1.045$.

The selected Ω_c, Ω_b, h, n_s are fine. Figures 5 show that the requirement is met also by w. On the contrary, Figures 6 show that the σ_8 value, tuned to observational data, lays outside the range considered at any z, for both $\mathcal{M}$ models.

This is most unfortunate. As we shall see the generalized expression in [13] will be scarcely useful to the present aims.

4. Numerical simulations

We shall compare simulations starting from realizations fixed by identical random seeds. Transfer functions generated using a modified version of the CAMB package [25] are

used to create initial conditions with a modified version of the PM software by Klypin & Holzmann [24], able to handle different parameterizations of DE [14, 28]. (Possible contributions from DE clustering on super–horizon scales are ignored in this work). Simulations were made by using two different programs: the ART code [26], courtesy of A. Klypin, and the PKDGRAV code [27], which has been modified to deal with any variable $w(a)$ for this work. The ART code has been mainly used as a benchmark to test our modified version of PKDGRAV (see appendix A); in the following we will only present results obtained with this latter code.

An important issue, when high accuracy is sought, is a suitable handling of cosmic (sample) variance. In order to address this point we create a series of simulations sharing the same box size and particle number, but with different realizations of the initial random density field.

The reference point are the simulations of the $\mathcal{M}$ models, performed in a box with side $L_{box} = 256h^{-1}$Mpc, a particle number $N = 256^3$ and a gravitational softening $\epsilon = 25h^{-1}$ kpc. We create 4 different realizations of them, only differing in the random seed used to sample the phase space. These initial conditions are then evolved from $z = 24$ to $z = 0$ and nine outputs are saved, at redshift z_k, from $z_0 = 2.4$ to $z_8 = 0$. For each redshift we then have the parameters, at $z = 0$, of the corresponding auxiliary $\mathcal{W}(z_k)$ model, as shown in Section 3. By using them we create suitable initial conditions for $\mathcal{W}(z_k)$ models, using the same random seed of the corresponding $\mathcal{M}$ model, and evolve the $\mathcal{W}(z_k)$ model down to z_k (9 redshift values z_k, 9 auxiliary models $\mathcal{W}(z_k)$ for each random seed). For instance, in order to build a spectrum expected to coincide with SUGRA at $z = 1.2$, we run a simulation of a constant–w model with $w = -0.7124$ and $\sigma_8 = 0.7351$ at $z = 0$.

4.1. Halos in simulations

Before reporting results on spectra and their evolution, we wish to exhibit a few results on halo formation. Since ever, mass functions have been considered a basic test for simulations. This is also an independent test going beyond spectral fits: spectra are related just to 2–point functions and their fitting formulae derive from theoretical elaborations on 2–point correlations; mass functions, instead, as the halo concentration distribution or the void probability, depend on convolutions of n–point correlations.

We look for virialized halos using a Spherical Overdensity (SO) algorithm. Candidate groups with a minimum of $N_f = 200$ particles are selected using a FoF algorithm with linking length $\phi = 0.2 \times d$ (the average particle separation). We then: (i) find the point C where the gravitational potential is minimum; (ii) determine the radius r of a sphere centered on C, where the density contrast is $\Delta_{\rm vir}$, with respect to the critical density of the Universe. Using all particles in the corresponding sphere we iterate the above procedure until we converge onto a stable particle set. For each stable particle set we obtain the virial radius, $R_{\rm vir}$, the number of particles within the virial radius, $N_{\rm vir}$, and the virial mass, $M_{\rm vir}$. We used a time varying virial density contrast

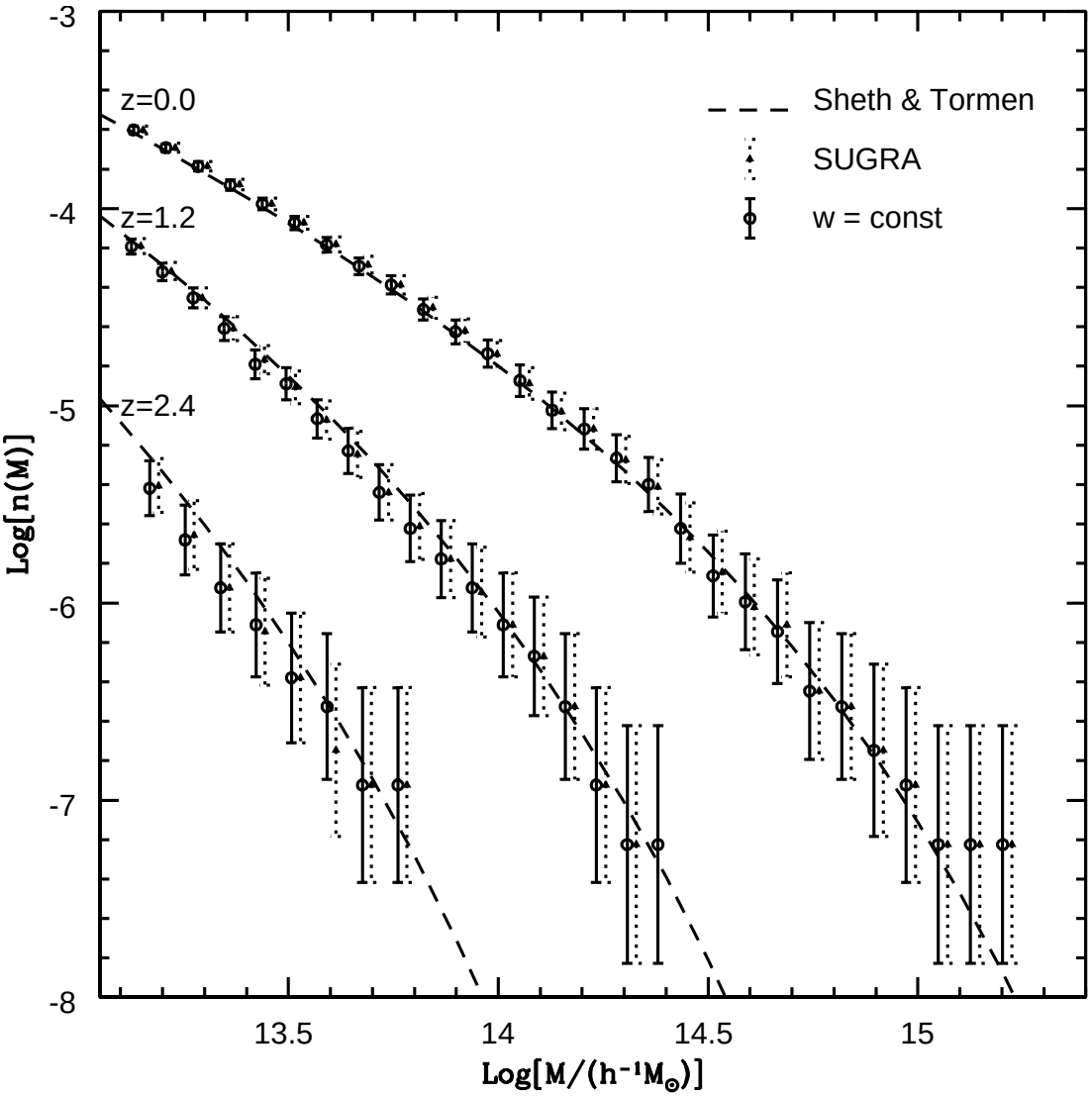

Figure 7. Number of halos per $(h^{-1}\mathrm{Mpc})^3$ in the SUGRA model considered and in the corresponding auxiliary $\mathcal{W}$ models. Results are practically undiscernable and in agreement with Sheth & Tormen expressions. The mass functions for the polynomial model behave quite similarly.

$\Delta_{\rm vir}$, whose value has been determined, according to linear theory, by using the fitting formulae in [28]. We include in the halo catalogue all the halos with more than 100 particles.

Mass functions are consistent with Sheth & Tormen predictions at all z, almost always within 2σ's (Poisson errors), while differences between $\mathcal{M}$ and $\mathcal{W}$ models can hardly be plotted. This allows us to formulate the conjecture that also higher order correlation functions coincide. As future cosmic–shear surveys will enable to inspect the 3–point function (and possibly to detect some higher order signal), we plan to compare n–point functions in $\mathcal{M}$ and $\mathcal{W}$ models, in a forthcoming paper.

5. Results on the Power Spectrum

Power spectra have been computed from N–body simulations by using the program PMpowerM of the ART package. The program works out the spectrum through a FFT (Fast Fourier Transform) of the matter density field, computed on a regular grid $N_G \times N_G \times N_G$ from the particle distribution via a CIC (Cloud in Cell) algorithm.

Figure 8, 9 and 10 present results on the Power Spectrum extracted from N–body simulations of the SUGRA model at $z = 0$, 0.6, 1.2, 1.8 and 2.4 . Their main significance is to allow a comparison between seeds and with Halofit expressions. The success of the *weak requirement* approach is so complete, that differences between SUGRA and its $\mathcal{W}$ models cannot be appreciated, even in the lower panel, where we report the ratio between spectra from simulations and fitting formulae. The situation is similar for the polynomial model (not plotted). Residual differences between $\mathcal{M}$ and $\mathcal{W}$ models will be shown in a following plot. Here, different colors refer to two different realizations,

The first Figure 8 shows a rather good fit with Halofit expressions at $z = 0$. Here we have another problem, which must be deepened by using simulation in a bigger bix and with a wider dynamical range; in fact, the differences between realizations are $< 1\,\%$ only for $k >\sim 3/h\mathrm{Mpc}^{-1}$ (where hydrodynamics becomes essential to describe the real world) and mostly keep within $2\,\%$ for $k >\sim 0.6/h\mathrm{Mpc}^{-1}$. At still lower k's, the seed dependence becomes more and more significant. A tentative explanation of the effect is that the relevant long wavelengths are still not sampled well enough, in a box of the size considered in this work, to yield a seed independent description at $z = 0$, when spectral contribution from long wavelengths had enough time to propagate down to such high wavenumbers.

In fact, already at $z = 0.6$ seed discrepancies $> 1\,\%$ are circumscribed to $k <\sim 0.6/h\mathrm{Mpc}^{-1}$. On the contrary, at this redshift, the discrepancy from Halofit steadily exceeds 4–5 % .

Higher redshift plots show a progressive deterioration of the Halofit expressions, which become unsuitable in the whole non–linearity range. No surprise about that, however, Halofit was built to meet ΛCDM spectra and its performance in the cases considered here is better than expected.

One could presume that using the expressions [13], aimed to fit $w \neq -1$ cosmologies, could allow some improvement. As well as Halofit, they are out of their range, but they include terms just aimed to correcting for $w \neq -1$. Unfortunately, they yield no improvement. As an example, in Figure 11, we plot spectral ratios at $z = 1.2$.

Let us now pass to the basic topic of this work and discuss discrepancies between $\mathcal{M}$ and $\mathcal{W}$ models. To this aim, it is useful to perform a preliminary comparison between the linear spectra. Figures 12 show spectral ratios for the polynomial and SUGRA models at redshift values distant 0.6 up to z=2.4 . For the polynomial model they can be confused with noise, apart of some extremely mild signal at low k ($\sim$ 1–2 : 100000). Low k discrepancies are greater (in the k range considered they are $\sim 1 : 10000$!) for SUGRA. Here we also appreciate a slight improvement from the FLL to our approach:

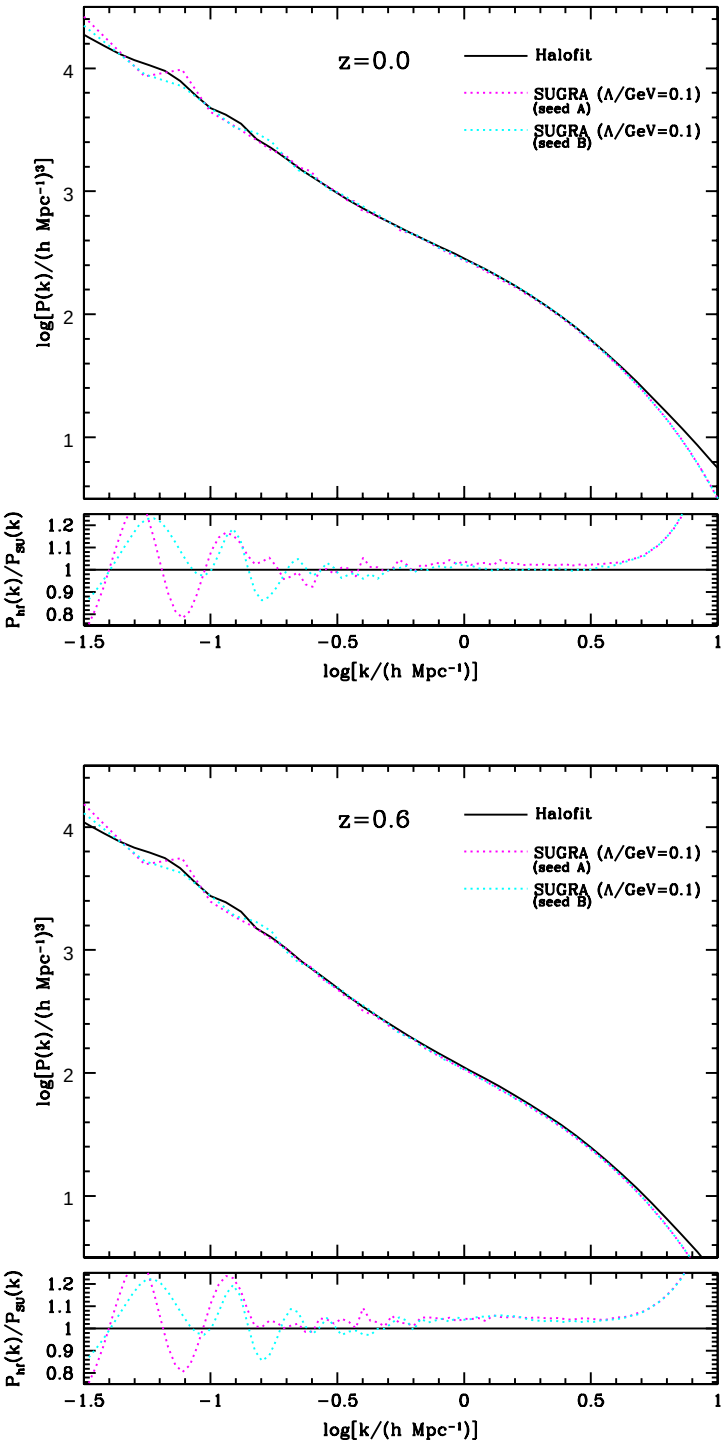

Figure 8. Spectra of SUGRA and auxiliary models at $z = 0$ and 0.6. Two realizations are shown. Differences between $\mathcal{M}$ and $\mathcal{W}$ models are so small to be unappreciable in these plots. In the lower frames, we rather exhibit the ratio with a Halofit expression, as well as the difference between realization. At $z = 0$, where $\mathcal{M}$ model spectra are quite close to ΛCDM, this is of the same order of the discrepancy from Halofit. At $z = 0.6$ the discrepancy from a Halofit expression already overcomes 5 % .

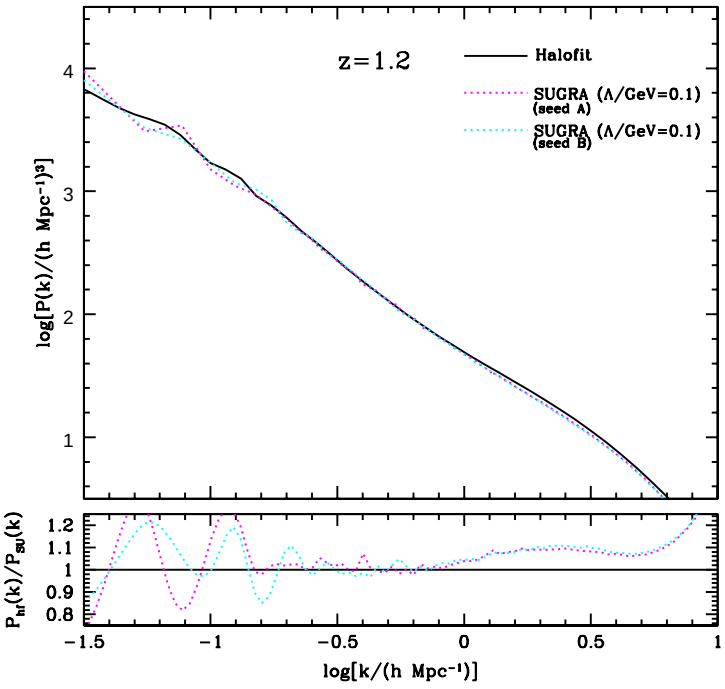

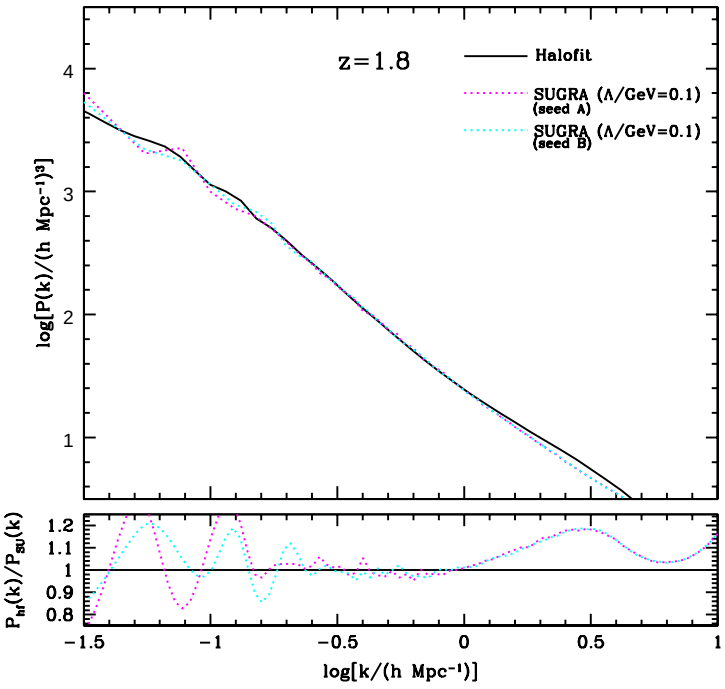

Figure 9. As Fig. 8, for $z = 1.2$ and $z = 1.8$. Notice the gradual deterioration of Halofit, which becomes unsuitable on the whole non–linearity range.

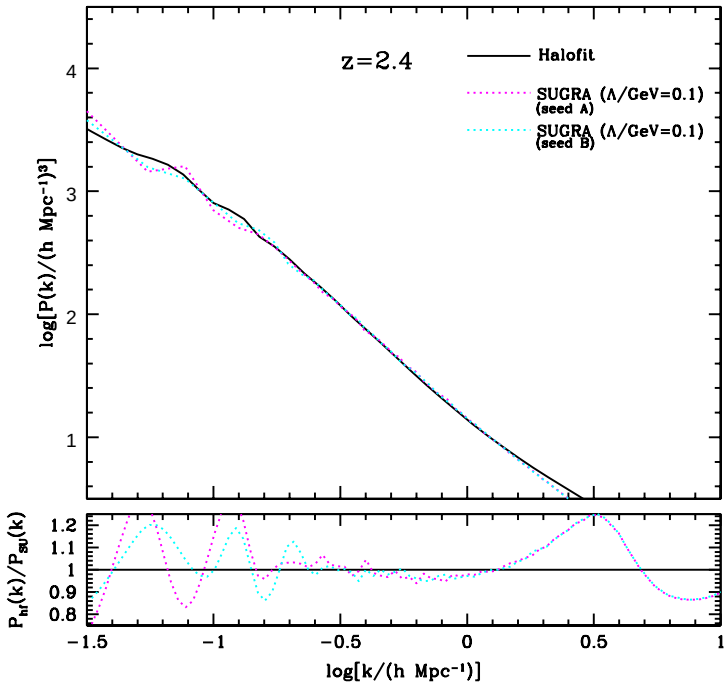

Figure 10. As Fig. 8, for $z = 2.4$. Discrepancies from Halofit exceed 20 % .

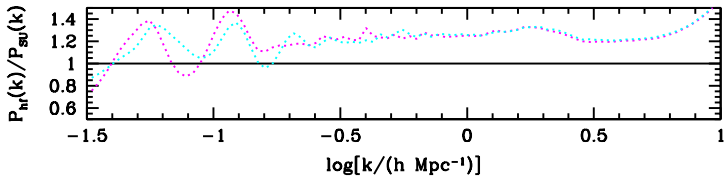

Figure 11. Comparison of spectra with the fitting expression with a correction for $w \neq -1$ [13], at $z = 1.2$. Quite in general, for our models, such expressions are no improvement in respect to Halofit (notice that the ordinate range has doubled). This is not unexpected, as they are used out of the allowed parameter range

in the former case, all spectra concern the same model, with the w value deduced for $z = 0$; in the latter one, we use a z–dependent w. But, at this discrepancy level, the main point to appreciate is that the linear spectra of $\mathcal{W}(z_k)$ are quite a good fit of the linear spectra of $\mathcal{M}$ at z_k.

The main results of this work are then described in the Figures 13 and 14. Let us remind that the polynomial model is one of those already considered by FLL, selected for the sake of comparison. As could also be expected from the linear spectra, both techniques perform better for this model, while the SUGRA model puts a more severe challenge.

In Figure 13 we show the ratio between power spectra for the polynomial model and the corresponding $\mathcal{W}(z_k)$ models. The spectra worked out by using the W.R. technique are given by solid lines. We also plot those obtained according to FLL (dashed lines).

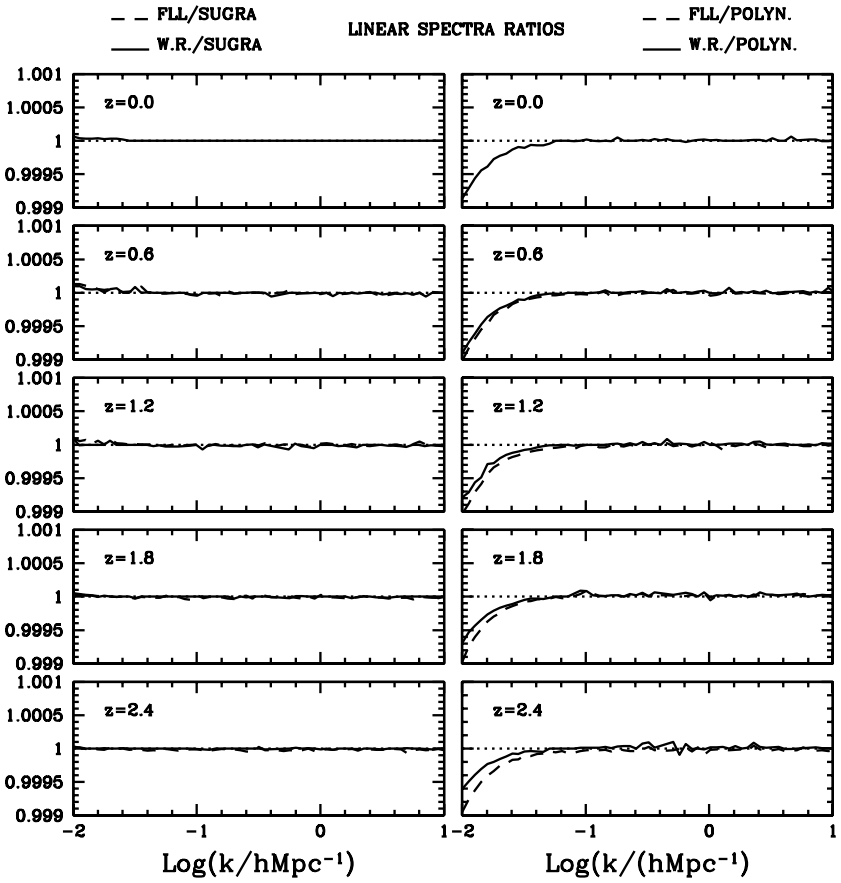

Figure 12. Linear spectra ratios.

Although spectra for two model realizations are plotted, their differences can hardly be appreciated.

Then, in Figure 14 we also show the ratio between power spectra for the SUGRA model and the corresponding auxiliary models $\mathcal{W}(z_k)$. Differences between model realizations are more easily appreciable here, than in the Figure 13 , but still quite negligible. What is immediately visible, instead, is the greater difficulty that both W.R. and FLL techniques have to approach SUGRA spectra.

Two different limitations are to be considered, when using such techniques. The first one arises from hydrodynamics and related effects. At $z = 0$ hydrodynamics pollutes N–body spectra when $k/h\mathrm{Mpc}^{-1}$ overcomes ~ 3: the number of halos with mass $> (4\pi/3)\ 3^3 \times 2.78 \cdot 10^{11} \Delta_{vir} M_\odot h^{-1}$ is enough to induce a spectral distortion $> 1\,\%$. At greater redshift, the same number of halos can be found only on smaller scales. Accordingly, N–body results are safe from hydro–pollution up to an increasing value of k. It is sufficient to look at Figure 7 to appreciate the scaling of the limiting value, which (in $h\mathrm{Mpc}^{-1}$ units) will be ~ 6 at $z \simeq 1.2$ and ~ 8 at $z \simeq 2.4$.

The second limitation is the one we test here. Possible differences between the spectra of the models $\mathcal{M}$ and $\mathcal{W}(z)$, at the redshift z, can arise from the different $a(t)$ history in the two models, after the non–linearity onset. Such differences shall be greater

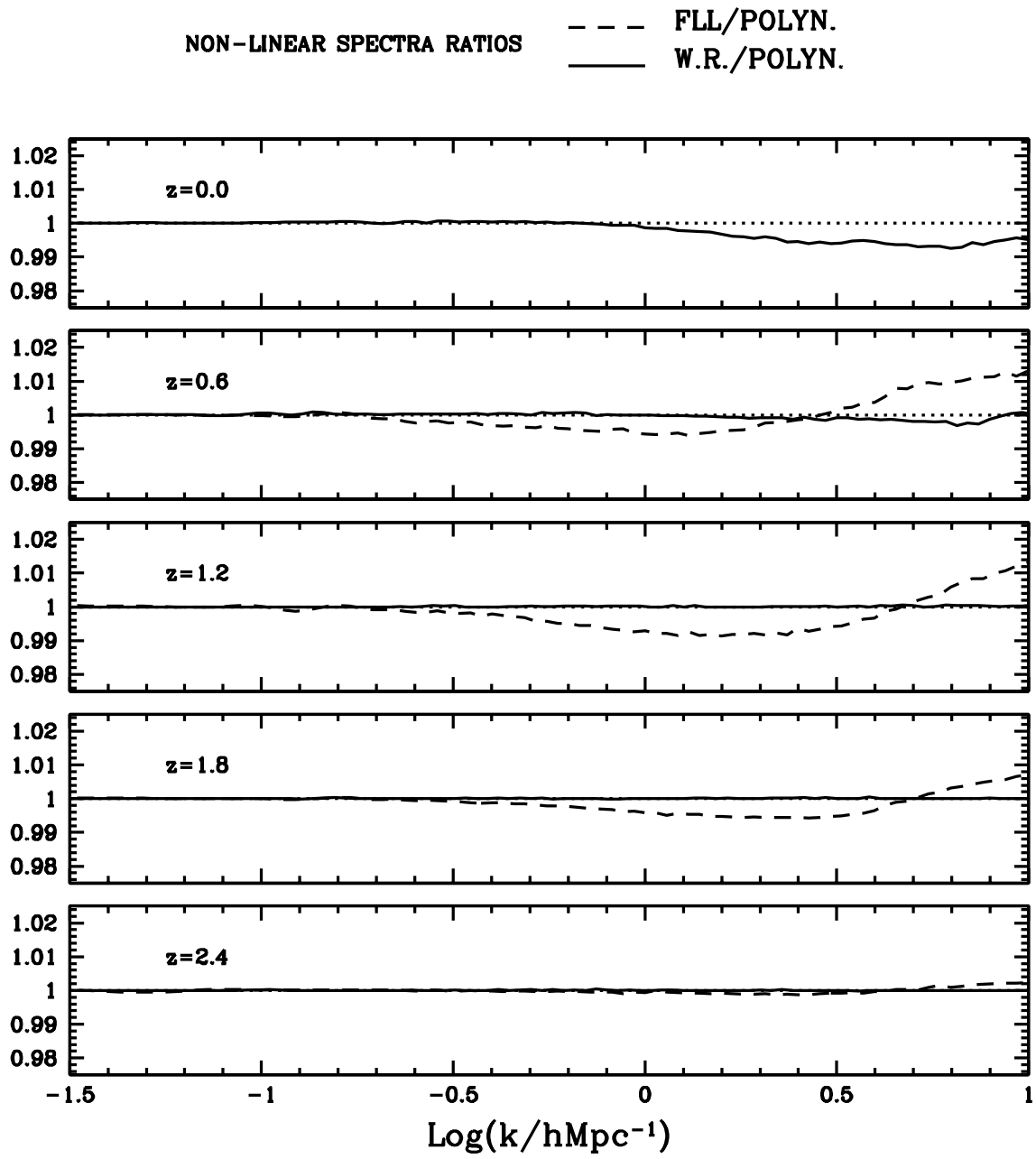

Figure 13. Ratio between power spectra for the polynomial model and the corresponding auxiliary models; dashed (solid) lines are obtained by using FLL (our) technique. Spectra for two model realizations are plotted, but differences are just marginally appreciable for the dashed lines. Up to $k = 3\,h\mathrm{Mpc}^{-1}$, the FLL approach already provides results with discrepancies within 1 %. They are smallest at $z = 2.4$, a redshift close to crossover. By using the weak requirement (W.R.) technique described in this work, the maximum discrepancies occur at $z = 0$, where they are presumably caused by the different non–linear history in $\mathcal{M}$ and $\mathcal{W}$ models, propagating its effects even below $k = 3\,h\mathrm{Mpc}^{-1}$. At $z = 0.6$ there is a residual discrepancy peaking at a value $\sim 0.3\,\%$ on a wavenumber $k \simeq 7\,h\mathrm{Mpc}^{-1}$. Otherwise, discrepancies keep within a fraction of permil, at any k.

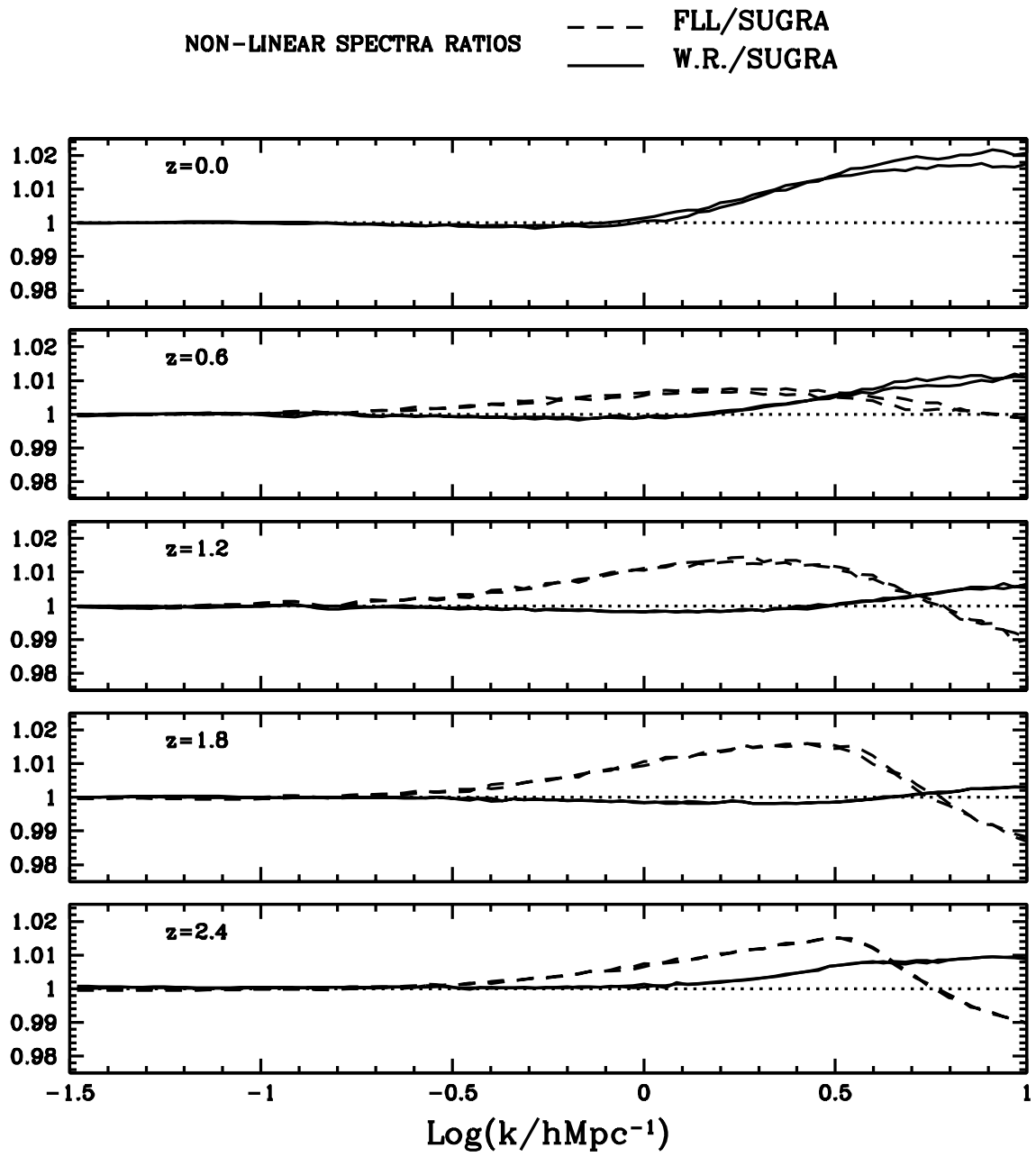

Figure 14. Ratio between power spectra for the SUGRA model and the corresponding auxiliary models; dashed and solid lines as in previous Figure. Again spectra for two model realizations are plotted and some slight differences are appreciable. At $z = 0$, where FLL and W.R. approaches coincide, differences between $\mathcal{M}$ and $\mathcal{W}$ models keep within 1% just up to $k = 1.8\,h\mathrm{Mpc}^{-1}$; at $k = 3\,h\mathrm{Mpc}^{-1}$, they are $\sim 1.3\,\%$. At higher redshift, the FLL technique provides discrepancies within $1\,\%$ just at $z = 0.6$. The W.R. technique here yields a great improvement, keeping discrepancies within $0.6\,\%$, $0.1\,\%$ $0.2\,\%$ $0.6\,\%$ at $z = 0.6$, 1.2, 1.8, 2.4, respectively.

on greater k (smaller scales), which became non–linear earlier. At a fixed k, differences in the non–linearity history will become more and more significant at later times.

These discrepancies are those we try to minimize and are shown in Figures 13, 14 . In the k range considered, they are already practically absent at $z = 0.3$, when using the W.R. approach. This is shown by all plots for $z \neq 0$ in the above two Figures. Here, the critical k for hydro distortions is systematically below the k where the non–linear history begins to matter. Just at $z \simeq 0$ the two critical k's are close, their relative setting being somehow model dependent.

Accordingly, while the spectra of the polynomial model, also treated by FLL, are easily met by the relative $\mathcal{W}$ model at $z = 0$, SUGRA confirms to be a harder challenge. Figures 13 and 14 however show that the W.R. technique is successful at any z, mostly attaining a precision at the per mil level, and hardly exceeding the 1 % discrepancy even in the most difficult cases.

6. Conclusions

By using the *"weak requirement"* condition described in this paper, we showed that even spectra of models with rapidly varying $w(a)$ are easily obtainable from constant–w spectra. We also verify that available *Halofit* expressions are not a sufficient approximation, already at $z \simeq 0.6$. Such expressions were generalized to $w =$ const. models by [13], but for a range of values of σ_8 which do not cover our case, tuned on recent observational outputs.

In our opinion, this means that strong efforts are soon to be made to provide generalized Halofit expressions, for constant–w models, effective for the whole parameter range that recent observations suggest to inspect, and working up to reasonably high redshift.

Let us then suppose that such expressions are available and that new observations provide direct information on density fluctuation spectra at N redshifts z_k ranging from 0 to z_N. Such spectra should then be fit to models, directly assuming that the reduced density parameters

$$\omega_c(z_k) = \omega_{o,c}(1 + z_k)^3 \ , \qquad \omega_b(z_k) = \omega_{o,b}(1 + z_k)^3 \ , \tag{4}$$

as it must however be, and seeking suitable w_k, $\sigma_8^{(z_k)}$, h_k. Using then each w_k, the $z = 0$ values $\sigma_{o,8}^{(z_k)}$ and $h_{o,k}$ should be easily reconstructed. The z_k dependence of w_k, $\sigma_{o,8}^{(z_k)}$, $h_{o,k}$ should then allow to recover a physical $w(z)$ behavior.

Let us outline, in particular, that the w_k values directly measured are not the physical $w(z)$. On the contrary, they can be quite far from it, as is made clear in Figure 5: there, the measured w_k correspond to the solid curves, while the physical state parameter scale dependence is given by the dotted curves.

The simultaneous use of the information on $\sigma_{o,8}^{(z_k)}$ (fitting curves similar to those in Figure 6, where it is simply named σ_8) and $h_{o,k}$ (which can be easily determined through linear programs), can allow a complete exploitation of forthcoming data.

Preliminary evaluations on the possible efficiency of observational techniques probing high redshift spectra, as the planned DUNE–EUCLID experiment, should be reviewed and possibly improved on the basis of the above conclusions.

Acknowledgments

Thanks are due to Anatoly Klypin and Gustavo Yepes for wide discussions. We are indebted with Joachim Stadel for granting us the use of the PKDGRAV code. We are also indebted with Giuseppe La Vacca for allowing us Figure 1, before its publication. Most numerical simulations were performed on the PIA cluster of the Max-Planck-Institut für Astronomie at the Rechenzentrum in Garching. Finally, it is a pleasure to thank an anonymous referee whose suggestions allowed us to improve and complete the presentation of our results. The support of ASI (Italian Space Agency) through the contract I/016/07/0 "COFIS" is acknowledged.

Appendix A. PKDGRAV and Dynamical Dark Energy

The central structure in PKDGRAV is a tree structure which forms the hierarchical representation of the mass distribution. Unlike the more traditional oct-tree PKDGRAV uses a k–D tree, which is a binary tree. The root-cell of this tree represents the entire simulation volume. Other cells represent rectangular sub-volumes that contain the mass, center-of-mass, and moments up to hexadecapole order of their enclosed regions. PKDGRAV calculates the gravitational accelerations using the well known tree-walking procedure of the Barnes-Hut algorithm [31]. Periodic boundary conditions are implemented via the Ewald summation technique [32]. PKDGRAV uses the ordinary time t (in suitable units) as independent variable. The link between the expansion factor a and the ordinary time t, in the case (Λ)CDM models is based on the equation:

$$\dot{a}/a = H(t) = (H_0 a^{-2})(\Omega_r + \Omega_m a + \Omega_\kappa a^2 + \Omega_\Lambda a^4)^{1/2} \tag{A.1}$$

where all the density parameters indicate redshift zero values. Herefrom one obtains soon that

$$t = \int_0^a da/\{aH(a)\} = (2/3)\int_0^{Y(a)} dy/\{yH[a(y)]\} \tag{A.2}$$

with

$$Y(a) = a^{3/2},\ a(y) = y^{2/3} \tag{A.3}$$

and the change of variable is clearly tailored on models based on CDM. All this procedure is modified in our algorithm. The program now creates *a priori* the $t(a)$ dependence, by integrating a suitable set of differential equations. A large number (~ 10000) of $t(a)$ values are then kept in memory and interpolated to work out $t(a)$ at any a value needed during the simulation run.

References

[1] Astier P *et al.* , 2006 *Astronom. Astrophys.* **447** 31
[2] Riess A G *et al.* , 2007 *Astrophys. J.* **659** 98
[3] Komatsu E *et al.* , 2008 *Preprint* 0803.0547v1.
[4] Cole S *et al.*, *Mon. Not. R. Astron. Soc.* **362**, 505 (2005).
[5] La Vacca G *et al.* in preparation
[6] Amendola L, Gasperini M and Ungarelli C, 2008 *Phys. Rev.* D **77** 123526
[7] Refregier A *et al.* , 2008 *Preprint* 0802.2522
[8] Huterer D and Tanaka M, 2005 *Astrophys. J.* **23** 369
[9] White S, 2004 *KITP Conf.: Galaxy-Intergalactic Medium Interactions* Kavli Institute for Theoretical Physics
[10] Jing Y P, Zhang P, Lin W P, Gao L and Springel V, 2006 *Astrophys. J.* **640** 119
[11] Rudd D, Zentner A and Kravtsov A, 2008 *Astrophys. J.* **19** 672
[12] Smith R E, Peacock J A, Jenkins A, White S D M, Frenk C S, Pearce F R, Thomas P A, Efstathiou G and Couchman H M P, 2003 *Mon. Not. R. Astron. Soc.* **341** 1311
[13] McDonald P, Trac H and Contaldi C, 2006 *Mon. Not. R. Astron. Soc.* **366** 547
[14] Klypin A, Macciò A V, Mainini R and Bonometto S A, 2003 *Astrophys. J.* **599** 31
[15] Macciò A V, Quercellini C, Mainini R, Amendola L, Bonometto S A, 2004 *Phys. Rev.* D **69** 123516
[16] Linder E V and Jenkins A, 2003 *Mon. Not. R. Astron. Soc.* **346** 573
[17] Solevi P, Mainini R, Bonometto S A, Macciò A V, Klypin A and Gottlber S, 2006 *Mon. Not. R. Astron. Soc.* **366** 1346
[18] Francis M J, Lewis G F and Linder E V, 2007 *Mon. Not. R. Astron. Soc.* **380** 1079
[19] Linder E and White M, 2005 *Phys. Rev.* D **72**, 061394
[20] Brax P H and Martin J, 1999 *Phys. Lett.* B **468** 40
[21] Brax P H and Martin J, 2001 *Phys. Rev.* D **62** 10350
[22] Brax P, Martin J and Riazuelo A, 2000 *Phys. Rev.* D **61** 103505
[23] Spergel D N *et al.* , 2007 *Astrophys. J. Suppl.* **170** 377
[24] Klypin A and Holtzman J, 1997 *Preprint* astro-ph/9712217
[25] Lewis A, Challinor A and Lasenby A, 2000 *Astrophys. J.* **538** 473
[26] Kravtsov A, Klypin A and Khokhlov A, 1997 *Astrophys. J. Suppl.* **111** 73
[27] Stadel J G, 2001 *PhD thesis* University of Washington
[28] Mainini R, Macciò A V, Bonometto S A and Klypin A, 2003 *Astrophys. J.* **599** 24
[29] Crocce, M., & Scoccimarro, R. 2008, *Phys. Rev.* D, **77**, 023533
[30] Colombo L and Gervasi M, 2006 *J. Cosmol. Astropart. Phys.* **10** 001
[31] Barnes J and Hut P, 1986 *Nature* **324** 446
[32] Hernquist L, Bouchet F, and Suto Y, 1991 *Astrophys. J. Suppl.* **75** 231